Available online at www.sciencedirect.com
ScienceDirect
Ceramics International 35 (2009) 1529–1538
CERAMICS INTERNATIONAL
www.elsevier.com/locate/ceramint

Structure and crystallization behaviour of some $MgSiO_3$-based glasses

Ashutosh Goel [a,b], Dilshat U. Tulyaganov [a,c], Essam R. Shaaban [d], Christopher S. Knee [e], Sten Eriksson [b], José M.F. Ferreira [a,*]

[a] Department of Ceramics and Glass Engineering, University of Aveiro, CICECO, 3810-193 Aveiro, Portugal
[b] Environmental Inorganic Chemistry, Chalmers University of Technology, SE-412 96 Gothenburg, Sweden
[c] State Committee of Geology and Mineral Resources, Centre of Remote Sensing and GIS Technologies, 11-A, Shevchenko Street, 100060 Tashkent, Uzbekistan
[d] Physics Department, Faculty of Science, Al-Azhar University, Assuit 71542, Egypt
[e] Department of Chemistry, University of Gothenburg, SE-412-96 Gothenburg, Sweden

Received 5 June 2008; received in revised form 11 July 2008; accepted 20 August 2008
Available online 30 September 2008

Abstract

We report on the structure and crystallization behaviour of four enstatite based glasses. Two glasses with nominal compositions of $Y_{0.125}Mg_{0.875}Si_{0.875}B_{0.125}O_3$ and $Y_{0.125}Mg_{0.725}Ba_{0.15}Si_{0.875}B_{0.125}O_3$ were prepared as parent glasses while the other two glasses were derived by the addition of 8 wt.% Al_2O_3 to the parent glass compositions, respectively. Structural features of the glasses were accessed by Fourier transform infrared spectroscopy (FTIR). Non-isothermal crystallization kinetics and thermal stability of Al_2O_3-free glasses were studied using differential scanning calorimetry (DSC). It has been shown that these glasses exhibit higher activation energy of viscous flow and are prone to surface crystallization. Activation energy of crystallization decreases with the addition of BaO in the glasses. Crystallization behaviour of all the experimental glasses in the temperature range of 800–1000 °C was followed by X-ray diffraction (XRD) and FTIR. Clinoenstatite and orthoenstatite were the major crystalline phases in the BaO-free glass-ceramics while BaO-containing compositions featured the early formation and stabilization of protoenstatite.

Keywords: A. Sintering; D. Glass; D. Glass-ceramics; D. Silicate

1. Introduction

Ceramic and glass-ceramic (GC) materials based on magnesium metasilicates ($MgSiO_3$) are ideal for high frequency low loss high voltage insulators, surge arrestors, standoffs, spacers, resistor and coil forms due to their good mechanical and low loss electrical properties. According to the review of Smith [1] and later by Lee and Heuer [2], $MgSiO_3$ occurs in three well characterized structures. Orthoenstatite (OE) and protoenstatite (PE) have orthorhombic symmetry while clinoenstatite (CE) has monoclinic symmetry. The character of $MgSiO_3$ polymorphism is complicated and changes from one form to another depending on temperature, pressure, dopants, internal stresses in grains and grain sizes [3–5]. It has been well documented in literature that during a thermal cycle OE transforms to PE, which is a stable polymorph of $MgSiO_3$ at temperatures $\geq$1000 °C; while during cooling PE crystallites invert to CE leading to the negative volume changes and thus, formation of intrinsic stresses in the ceramic body which further causes the deterioration of steatite ceramics [2]. Mielcarek et al. [5] demonstrated that after 250 h of conditioning at room temperature the bending strength of PE based specimens was twice less than at the beginning. Therefore, the quality of steatite ceramics is strictly correlated with the degree of PE to CE inversion [5].

The production of $MgSiO_3$-based materials via GC route features particular peculiarities because the precise stoichiometric composition of enstatite does not result in a stable glass. Lee and Heuler [2] attempted to produce stoichiometric $MgSiO_3$ glass by quenching the glass melt in the water through which liquid N_2 was bubbling. Heat treating a powder from that glass with an average particle diameter of about 180 μm between 800 °C and 1000 °C caused crystallization of OE, which was invariably associated with CE, independent of annealing time and cooling conditions (air, water, or slow

* Corresponding author. Tel.: +351 234 370242; fax: +351 234 370204.
E-mail address: jmf@ua.pt (J.M.F. Ferreira).

0272-8842/$34.00
doi:10.1016/j.ceramint.2008.08.012

cooling of 5 K/min). At temperatures ≥1200 °C, formation of PE at the expense of OE was observed while CE was formed during cooling. The sintered GC samples were highly porous, even after many hours of heat treatment at temperatures close to melting point.

In our previous study [6], we experimentally determined the influence of Al_2O_3 on sintering and crystallization behaviour of enstatite based glass powder compacts. Two glasses with nominal compositions of $Y_{0.125}Mg_{0.875}Si_{0.875}B_{0.125}O_3$ and $Y_{0.125}Mg_{0.725}Ba_{0.15}Si_{0.875}B_{0.125}O_3$ were prepared by melt-quenching technique. With respect to $MgSiO_3$, in the first ($Y_{0.125}Mg_{0.875}Si_{0.875}B_{0.125}O_3$) and in the second ($Y_{0.125}Mg_{0.725}Ba_{0.15}Si_{0.875}B_{0.125}O_3$) glass compositions, substitutions of yttrium and barium for magnesium as well as boron for silicon were attempted. Further, two more glasses with the addition of 8 wt.% Al_2O_3 in both the parent glasses, respectively, were prepared. The addition of Al_2O_3 in the glasses decreased dilatometric glass transition temperature (T_{dg}) and softening temperature (T_{ds}) and increased the difference between T_c (onset temperature of crystallization) and T_{dg}, thus, resulting in well sintered $MgSiO_3$-based glass-ceramics of high quality. On the contrary, the parent Al_2O_3-free glass powder compacts showed poor sintering ability in the temperature range 900–1100 °C. The presence of Al_2O_3 stabilized CE and OE in the BaO-free $MgSiO_3$ GCs. However, the presence of BaO favoured the early formation (≥900 °C) of PE in the Al_2O_3-free GCs and hexacelsian formation in the Al_2O_3-containing GCs.

Despite the very interesting features reported above, literature survey reveals that $MgSiO_3$-based glasses and GCs have received less attention and hence poor documentation. Therefore, in order to gain an in-depth knowledge of the phase relationships in the enstatite based GCs, the present work is a logical sequel to our previous study [6] aiming at investigating the structural features and crystallization kinetics of $MgSiO_3$-based glasses.

2. Experimental

Al_2O_3-free parent glass compositions $Y_{0.125}Mg_{0.875}Si_{0.875}B_{0.125}O_3$ (designated as 2a) and $Y_{0.125}Mg_{0.725}Ba_{0.15}Si_{0.875}B_{0.125}O_3$ (designated as 3a); and Al_2O_3-containing glasses named as 2b and 3b derived from compositions 2a and 3a, respectively, by adding 8 wt.% Al_2O_3 (Table 1) were prepared and examined. The incorporation of NiO (1 wt.%) in the batches was considered to improve the adhesion of the resultant GCs to the metals for further technological applications. Powders of technical grade SiO_2 (purity >99.5%) and of reactive grade Al_2O_3, H_3BO_3, MgO, Y_2O_3, $BaCO_3$, and NiO were used. Homogeneous mixtures of batches (~100 g), obtained by ball milling, were preheated at 900 °C for 1 h for calcination and then melted in platinum crucibles at 1600 °C for 1 h, in air. Glasses in bulk form were produced by casting of melts onto preheated bronze moulds and subsequent immediate annealing at 550 °C for 1 h. Glasses in frit form were obtained by quenching of the melts in cold water. The frit was dried and then milled in a high-speed porcelain mill to obtain fine powders. The measured mean particle size of the experimental glass powders, determined by light scattering technique (Coulter LS 230, UK, Fraunhofer optical model), was in the range of 2.8–3.0 μm.

Table 1
Compositions of batches of the investigated glasses.

Glass		MgO	BaO	SiO_2	B_2O_3	Al_2O_3	Y_2O_3	NiO
2a	wt.%	32.83	–	48.96	4.05	–	13.14	1.00
	mol%	46.30	–	46.32	3.31	–	3.31	0.76
2b	wt.%	30.21	–	45.05	3.73	8.00	12.09	0.92
	mol%	44.16	–	44.18	3.16	4.62	3.15	0.73
3a	wt.%	23.46	18.46	42.22	3.48	–	11.33	1.00
	mol%	38.33	7.93	46.27	3.29	–	3.30	0.88
3b	wt.%	21.59	16.99	38.85	3.21	8.00	10.44	0.92
	mol%	36.29	7.51	43.80	3.12	5.32	3.13	0.83

Infrared spectra of the glass powders and GCs were obtained using an infrared Fourier spectrometer (FTIR, model Mattson Galaxy S-7000, USA) in the range of 300–1500 cm^{-1}. For this purpose, each sample was mixed with KBr in the proportion of 1/150 (by weight) for 15 min and pressed into a pellet using a hand press.

Crystallization kinetics of the glass was studied using differential scanning calorimetry (DSC-TG, NETZSCH STA 409 PC Luxx thermal analyzer) interfaced with a computerized data acquisition and analysis system. The glass powder weighing ~50 mg was contained in an alumina cup. The samples were heated, in flowing nitrogen atmosphere (20 mL/min), from ambient temperature to 1050 °C at heating rates (β) of 2, 5, 15 and 20 K/min. The value of the glass transition temperature T_g, crystallization onset temperature, T_c and peak temperature of crystallization, T_p were obtained from the DSC scans.

Dilatometry measurements were done with the prismatic samples of annealed bulk glass blocks with cross section 4 mm × 5 mm at a heating rate of 5 K/min (Bahr Thermo Analyze DIL 801 L, Germany).

The GCs were prepared by powder processing route. The glass powders were granulated (by stirring in a mortar) in 5 vol.% polyvinyl alcohol solution (PVA, Merck; the solution of PVA was made by dissolution in warm water) in a proportion of 97.5 wt.% of powder and 2.5 wt.% of PVA solution. Rectangular bars with dimensions of 4 mm × 5 mm × 50 mm were prepared by uniaxial pressing (80 MPa). The green bars were sintered at different temperatures (800 °C, 900 °C and 1000 °C) in air. The soaking time at the sintering temperatures was 1 h, while a slow heating rate of 4 K/min was maintained in order to prevent deformation of the samples. The crystalline phases were identified by X-ray diffraction analysis (XRD, Cu $K\alpha_1$ radiation, Bruker AXS, D8 Advance, Germany) in the scan range of diffraction angles (2θ) between 10° and 80° with a 2θ-step of 0.02°/s. The phases were identified by comparing the experimental X-ray patterns to standards compiled by the International Centre for Diffraction Data (ICDD). FTIR was employed to investigate the structural changes in the GCs with respect to temperature.

3. Results and discussion

3.1. Preparation of glasses

For all the investigated compositions, melting at 1600 °C for 1 h was adequate to obtain bubble-free transparent glasses. Absence of any crystalline inclusions was confirmed by XRD and further by SEM analysis. The brown colour of the experimental glasses is probably due to the addition of NiO. Nickel is one of the elements that impart oxide glasses the widest range of colouration: green, yellow, brown, purple, and blue. These modifications of the glass colour have been interpreted in the past as arising from two kinds of sites, octahedral and tetrahedral, the proportion of which varies as a function of glass composition [7]. The origin of this brown colouration in the glasses is due to the presence of nickel in five-coordination, in trigonal bipyramids [8].

3.2. Structural features and crystallization kinetics of the investigated glasses

The room temperature FTIR transmittance spectra of the investigated glasses are shown in Fig. 1. All the spectra exhibit four broad transmittance bands in the region of 300–1500 cm^{-1}. The most intense bands lie in the 800–1300 cm^{-1} region, the next between 300 and 600 cm^{-1} and 1350–1500 cm^{-1}, while the least intensive lies between 650 and 800 cm^{-1}. This lack of sharp features is indicative of the general disorder in the silicate network mainly due to a wide distribution of Q_n units (polymerization in the glass structure, where n denotes the number of bridging oxygen) occurring in these glasses. The broad band in the 800–1300 cm^{-1} is assigned to the stretching vibrations of the SiO_4 tetrahedron with different number of bridging oxygen atoms [9,10]. For glasses 2a and 3a, this band is around 1050–1070 cm^{-1} indicating the distribution of Q_n units centred on the Q_3 and possibly Q_4, while for glasses 2b and 3b, this band shifts towards lower wave numbers with addition of Al_2O_3, implying towards the decease in the connectivity of the silicate glass network. According to Ojovan and Lee [11], introduction of boron in the silicate glasses leads to the breaking up of Q_3 units and the formation of Q_2, Q_4 and small amounts of Q_1 units. The transmittance band in the region 800–1300 cm^{-1} for glass 2a is centred around 1070 cm^{-1} while for BaO-containing glass (3a), it is centred at 1049 cm^{-1}. This shows that BaO effectively depolymerizes the silicate glass network. The bands in the 300–600 cm^{-1} region are due to bending vibrations of Si–O–Si linkages. The transmittance band in the 650–800 cm^{-1} region in the glasses 2a and 3a is attributed to the bending vibrations of bridging oxygen between trigonal boron atoms while in glasses 2b and 3b, it is also related to the stretching vibrations of the Al–O bonds with Al^{3+} ions in four-fold coordination. The band in the region 1350–1500 cm^{-1} corresponds to B–O vibrations in $[BO_3]$ triangle. Borate glasses show two characteristic bands derived from the B–O bonds in the $[BO_3]$ triangles (about 1300–1500 cm^{-1}) and the $[BO_4]$ tetrahedra (about 1000 cm^{-1}) [12]. These bands get shifted under the influence of surrounding cations, the extent and the direction of this shift depending on the type of cation. FTIR spectra of the glasses under investigation show that in these glasses boron primarily occurs in the form of $[BO_3]$ triangles (1396 cm^{-1}). However, the presence of $[BO_4]$ tetrahedron in the glass structure cannot be neglected. Since the IR band for $[BO_4]$ tetrahedron (about 1000 cm^{-1}) overlaps with that of stretching vibrations of SiO_4, therefore, it could not be observed in the present investigation. No other band could be resolved in the spectra of the glasses.

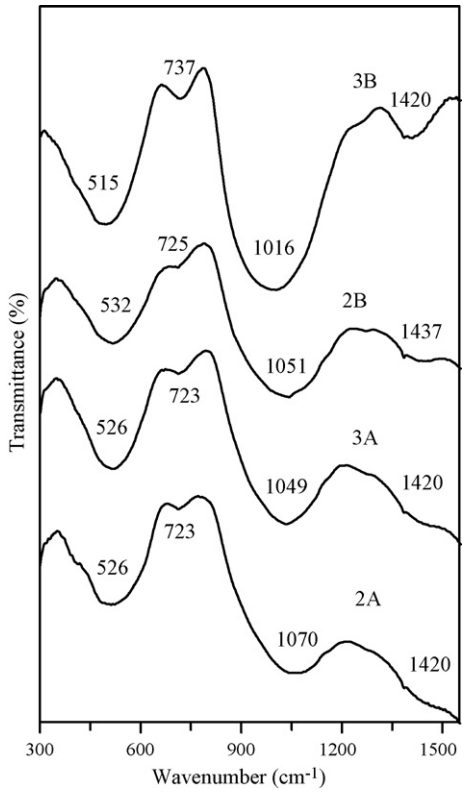

Fig. 1. FTIR spectra of the investigated glass powders.

The coefficient of thermal expansion (CTE) of the glasses was observed to decrease with the addition of Al_2O_3 in BaO-free glasses (2a and 2b) while it increased for glass 3b in comparison to glass 3a (Table 2). However, CTE for BaO-containing glasses (3a and 3b) was observed to be higher in comparison to BaO-free glasses (2a and 2b). Addition of BaO is known to increase the CTE of silicate glasses [13] as it favours the formation of non-bridging oxygens (NBO) in the silicate glass network (Fig. 1). The CTE of all the investigated glasses is lower than the clinopyroxene based diopside ($CaMgSi_2O_6$) – Ca – tschermak

Table 2
Thermal parameters obtained for the investigated glasses in our previous study [6] along with the CTE of the glasses.

Glass	T_{dg}[a] (K)	T_{ds}[a](K)	T_c[a](K)	T_p[a] (K)	$T_c - T_g$ (K)	CTE[a,b]
2a	943	983	1108	1135	165	7.14
2b	863	943	1143	1171	280	6.29
3a	943	971	1133	1163	190	7.19
3b	883	926	1168	1201	285	7.38

[a] $\beta = 5$ K/min.
[b] CTE × 10^6 K^{-1} (200 °C–500 °C).

($CaAl_2SiO_6$) (Di-Ca-Ts) glasses as reported in our earlier studies [13–15]. This may be attributed to the higher degree of polymerization in the silicate glass network of enstatite based glasses and also, to the presence of B_2O_3 in the glasses. According to Ojovan and Lee [11], B_2O_3 when present in less than 15 wt.%, decreases the CTE of the silicate glasses.

In our previous study [6], we observed that Al_2O_3 addition in the enstatite based glasses decreases the T_{dg}, and T_{ds} while the peak temperature of crystallization (T_p) was observed to shift towards higher temperature. The results from our previous study [6] along with the CTE of the investigated glasses are summarized in Table 2 for the convenience of readers. Consequently, addition of Al_2O_3 outstandingly improved densification of $MgSiO_3$-based glass powder compacts due to increase in the interval of sintering range between T_{dg} and onset temperature of crystallization (T_c). Completely dense samples with grey colour and smooth surfaces were obtained after heat treatment at 900 °C for 1 h. In contrast the glass powder compacts prepared from Al_2O_3-free compositions 2a and 3a exhibited poor sintering ability after heat treatment at 900 °C and 1000 °C. The resultant samples, of white colour, were highly porous and extensively fractured. The poor sintering ability of Al_2O_3-free compositions may be due to the occurrence of crystallization before or simultaneously with sintering stage, thus, leading to porous and heterogeneous material.

In quest for the reason behind poor sintering ability of Al_2O_3-free glasses, we investigated the non-isothermal crystallization kinetics and thermal stability of glasses 2a and 3a using DSC. Representative DSC thermographs for both the glasses (2a and 3a), taken at different heating rates (Fig. 2), exhibit an endothermic dip before the onset of crystallization and a single well defined crystallization exotherm. The values of glass transition temperature (T_g), T_c and T_p shifted towards higher side with increase in heating rate (Table 3). A slight decrease in T_g and increases in T_c and T_p were observed with the addition of BaO in the glasses. The decrease in T_g with the addition of BaO may be attributed to the depolymerization of the silicate glass network. The higher value of T_p for glass 3a is in accordance with our previous results [13], where T_p for BaO-free Di-Ca-Ts glass ($CaMg_{0.8}Al_{0.4}Si_{1.8}O_6$) was lower than its BaO-containing derivatives ($Ca_{0.95}Ba_{0.05}Mg_{0.8}Al_{0.4}Si_{1.8}O_6$; $Ca_{0.9}Ba_{0.1}Mg_{0.8}Al_{0.4}Si_{1.8}O_6$ and $Ca_{0.8}Ba_{0.2}Mg_{0.8}Al_{0.4}Si_{1.8}O_6$). In general, the T_p for enstatite based glasses, under present investigation, were observed to be lower than the diopside based glasses.

Since the densification of glass powder compacts is initially obtained through viscous flow at temperatures slightly higher than T_g, the activation energy of viscous flow occurring around glass transition (E_η) was calculated using the Eq. (1) [16,17]:

$$\ln\left(\frac{T_g^2}{\beta}\right) = \frac{E_\eta}{RT_g + \text{const.}} \quad (1)$$

where, β is the heating rate, R is the Gas constant. From Fig. 3 and Table 4, it is clear that glass 2a shows higher E_η in comparison to glass 3a. The E_η for glass 2a and 3a is much higher than for Al_2O_3-containing Di-Ca-Ts glasses investigated in our previous study ($CaMg_{0.8}Al_{0.4}Si_{1.8}O_6$, Di/Ca-Ts = 80/20;

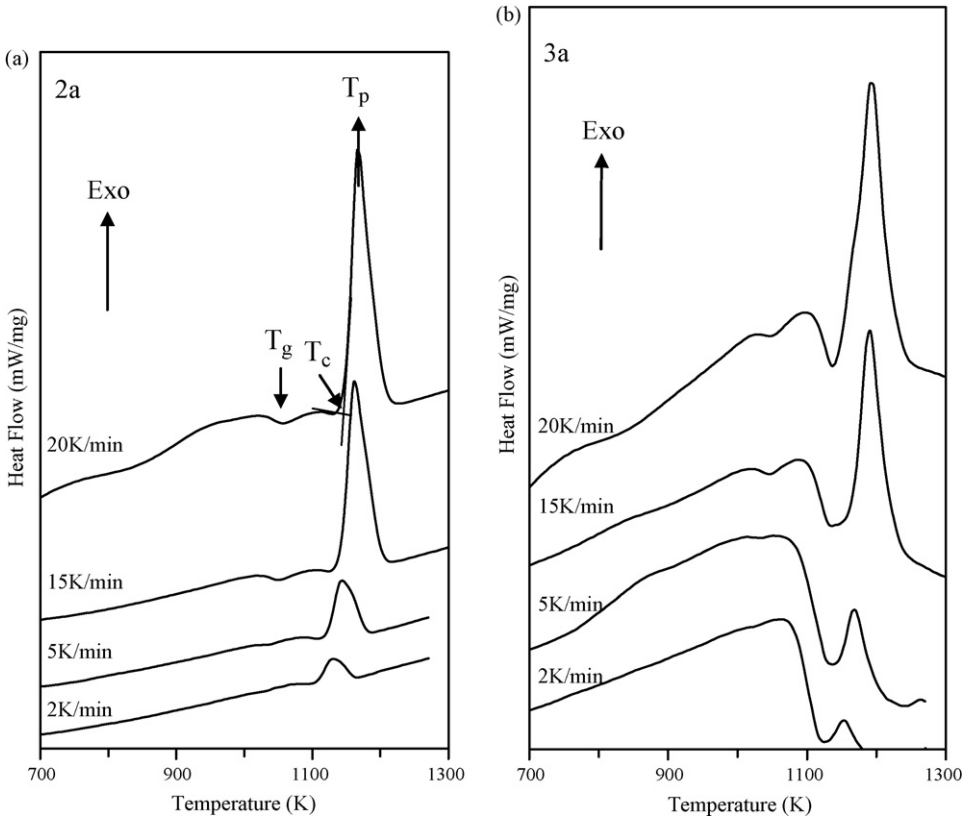

Fig. 2. Differential scanning calorimetry (DSC) thermographs of the glass powder (a) 2a and (b) 3a at different heating rates.

Table 3
Influence of heating rate of the thermal parameters of both the glasses.

Glass 2a					Glass 3a			
β (K min^{-1})	T_g (K)	T_c (K)	T_p (K)	Area[a] (J g^{-1})	T_g (K)	T_c (K)	T_p (K)	Area[a] (J g^{-1})
2	1031	1102	1131	219.2	1026	1131	1153	126.6
5	1040	1111	1145	233.7	1035	1140	1168	132.0
15	1056	1129	1161	249.0	1051	1156	1190	161.1
20	1061	1133	1166	252.7	1056	1158	1195	203.3

[a] Area under the crystallization curve of the DSC thermograph.

$CaMg_{0.75}Al_{0.5}Si_{1.75}O_6$, Di/Ca-Ts = 75/25; $CaMg_{0.7}Al_{0.6}Si_{1.7}O_6$, Di/Ca-Ts = 70/30 (mol%)) [18]. Moreover, it was observed in our previous study that E_η decreased with increasing the Al_2O_3 content in the glasses and the GCs obtained from Di-Ca-Ts glass powder compacts showed good sintering behaviour and exhibited high mechanical strength. Therefore, higher temperature is required to achieve good sintering in Al_2O_3-free enstatite glasses in comparison to Al_2O_3-containing glasses. However, at higher temperature, crystallization process starts, which further hinders the sintering of the glass powder compacts.

Further, as also mentioned in the introduction, enstatite based glasses are difficult to prepare. In fact, we too faced some serious difficulties in casting the glass with composition corresponding to 75% enstatite and 25% diopside, in our earlier study [19]. Therefore, glass-forming ability of the glasses 2a and 3a was determined by calculating the kinetic fragility index, F, because it is a measure of the rate at which the relaxation time decreases with increasing temperature around T_g and is given by Eq. (2) [20,21]:

$$F = \frac{E_\eta}{RT_g \ln 10} \tag{2}$$

According to Vilgis [22], glass-forming liquids that exhibit an approximate Arrhenius temperature dependence of their relaxation times are defined as strong and specified with low value of F ($F \approx 16$), while the limit for fragile glass-forming liquids is characterized by a high value of F ($F \approx 200$) [23]. As is evident from Table 4, glass 3a has slightly lower value of F in comparison to glass 2a. However, considering that the values of F for both the glasses are within the above mentioned limit, it is reasonable to state that both the glasses are obtained from strong glass-forming liquids. It is noteworthy that the value of F for the glasses under investigation is significantly higher in comparison to the clinopyroxene based Di-Ca-Ts glasses [18], which explains the cause of the difficulties met by us in preparing the enstatite based glasses in our previous study [19].

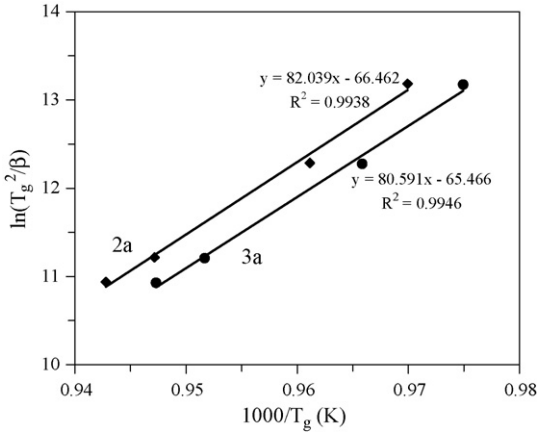

Fig. 3. Plot for determination of activation energy for viscous flow (E_η) for glasses 2a and 3a.

The crystallization kinetics of the glasses was studied using the formal theory of transformation kinetics as developed by Johnson and Mehl [24] and Avrami [25], for non-isothermal processes that has already been obtained in our previous work [26,27]:

$$\ln\left(\frac{T_p^2}{\beta}\right) = \frac{E_c}{RT_p} - \ln q = 0 \tag{3}$$

which is the equation of a straight line, whose slope and intercept give the activation energy, E_c, and the pre-exponential factor, $q = Q^{1/n}K_0$ (refer to Ref. [26]), respectively and the maximum crystallization rate by the relationship:

$$\left.\frac{d\chi}{dt}\right|_p = 0.37\beta E_c n (RT_p^2)^{-1} \tag{4}$$

which makes it possible to obtain, for each heating rate, a value of the kinetic exponent, n. In Eq. (4), χ corresponds to the crystallization fraction and $d\chi/dt|_p$ corresponds to the crystallization rate, which may be calculated by the ratio between the ordinates of the DSC curve and the total area of the crystallization curve. The graphical representation of the volume fraction crystallized for the exothermic curves of both the glasses shows a typical sigmoid curve as a function of temperature for different heating rates (Fig. 4).

Table 4
Thermal parameters showing the thermal stability and crystallization mechanism in both the glasses.

	2a	3a
E_η (kJ mol^{-1})	682	670
F[a]	34.55	34.12
$<n>$	1.07 ± 0.014	1.11 ± 0.017
q (s^{-1})	1.2×10^{30}	2.65×10^{24}
E_c (kJ mol^{-1})	718	604

[a] $\beta = 2$ K/min.

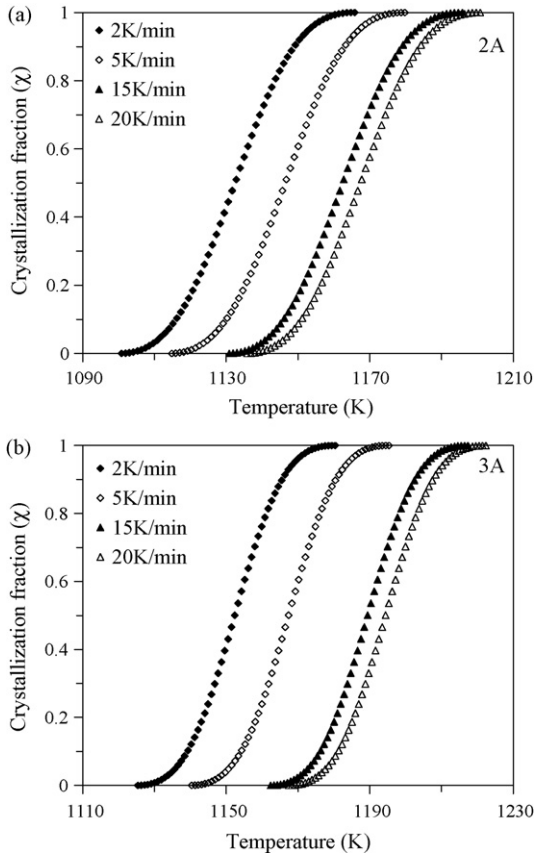

Fig. 4. Crystallization fraction (χ) *vs.* temperature (T) for the crystallization curve of glasses (a) 2a and (b) 3a.

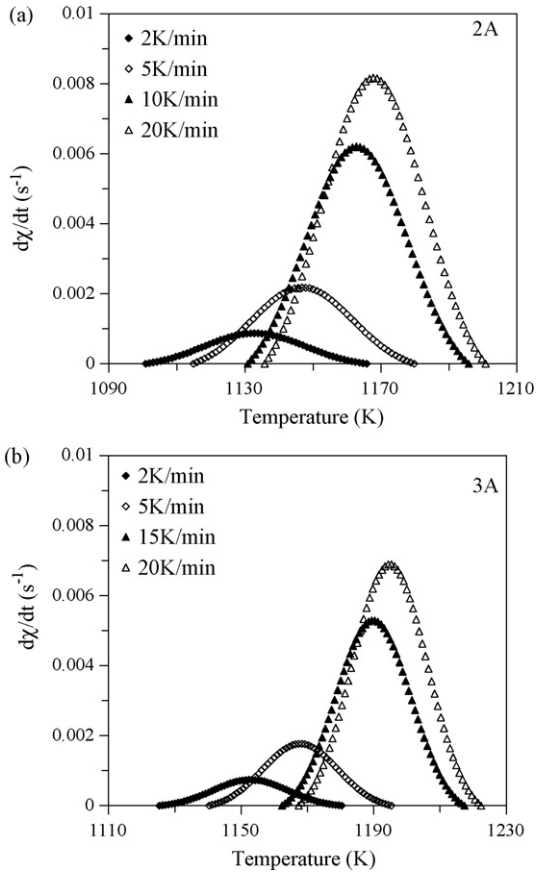

Fig. 5. Crystallization rate ($d\chi/dt$) *vs.* temperature (T) for the crystallization curve of glasses (a) 2a and (b) 3a.

It may be observed that the $d\chi/dt|_p$ value increases as well as the heating rate (Fig. 5), which has been discussed in literature [28]. The values of E_c and n for both the glasses are listed in Table 4 and presented in Fig. 6. The E_c value for glass 3a is considerably lower than glass 2a, while the value of n has been obtained to be near to 1 for both the glasses A value of n close to 3 supports bulk or three dimensional crystal growth and a value close to 1 indicates surface growth. Intermediate values of n between 1 and 3 might result when surface and internal crystallization occur simultaneously. Therefore, from the value of n, it is evident that surface crystallization predominates in both glasses. The lower E_c for glass 3a is in accordance with our previous results [13] and may be attributed to the presence of BaO, as this oxide tends to increase the crystalline volume fraction in silicate glasses. This is supported by the decrease in the area under the DSC crystallization curve for glass 3a in comparison to glass 2a at a particular heating rate (Table 3). In general, E_c for enstatite based glasses is higher in comparison to their diopside based counterparts [13,15,18].

3.3. Crystallization behaviour of glass powder compacts

In order to follow the crystalline phase assemblage in the resultant GCs at different temperatures, XRD data collected at room temperature (RT-XRD) from the sintered GCs in the present study was analyzed and is summarized in Table 5, along with the in situ high temperature XRD (HT-XRD) data obtained from our previous study [6]. It is noteworthy that the latter represents the revised and corrected version of the Table 4 documented in our previous study [6].

To be consistent with the work of Lee and Heuer [2], we have used the ICDD cards 00-019-0768 for OE and 00-011-273 for PE. ICDD card 00-035-0610 was used for CE instead of 00-019-0769 as the latter has been replaced by former in the new ICDD classification. It should be also mentioned that since the diffractograms of synthetic CE and OE are quite similar, we

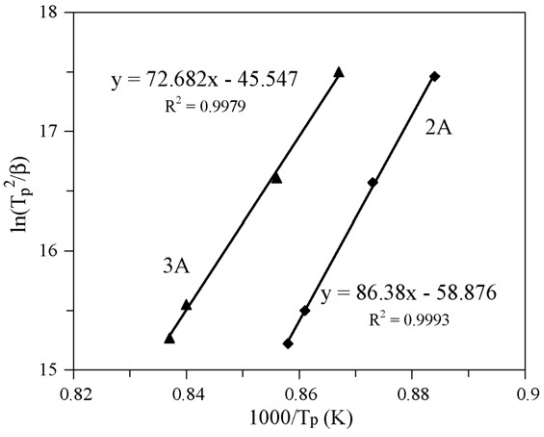

Fig. 6. Plot of activation energy for crystallization (E_c) for glasses 2a and 3a.

Table 5
Evolution of crystalline phases assemblages in the investigated glasses over increasing temperature, determined by the high temperature X-ray diffraction (HT-XRD) and room temperature X-ray diffraction (RT-XRD) analysis. (*Note*: The phases indicated are listed in the order of their decreasing intensities in the respective XRD spectra.).

Glass		800 °C	900 °C	1000 °C	1100 °C
2a	HT-XRD	–	CE, OE	CE, OE	CE, OE, PE, K
	RT-XRD	Amorphous with some CE and OE	CE, OE, Q	CE, OE, Q	–
2b	HT-XRD	–	CE, OE	CE, OE	–
	RT-XRD	Amorphous with some CE	CE, OE	CE, OE	–
3a	HT-XRD	–	PE, Q	PE, Q	PE, Q
	RT-XRD	Amorphous	CE, PE, YS, K	PE, YBSi, BaSi	–
3b	HT-XRD	–	HC, CE, OE, PE	HC, CE, PE, OE	–
	RT-XRD	Amorphous with some CE and HC	HC, CE, OE, PE	HC, CE, PE, OE	–

CE, clinoenstatite; OE, orthoenstatite; PE, protoenstatite; Q, quartz; YS, yttrium silicate; K, keivyite; HC, hexacelsian; YBSi, yttrium oxide borate silicate; BaSi, barium silicon oxide. (For ICDD card nos. and chemical formulas of the respective phases, please refer to the text.)

have considered the peak corresponding to $2\theta = 29.999^\circ$ for securing the presence of CE.

According to HT-XRD results, CE and OE precipitated in composition 2a at 900 °C and 1000 °C (Table 5), however, the intensity of the peaks slightly increased at 1000 °C. With further increase in temperature to 1100 °C, PE and keivyite (designated as K; $Y_2Si_2O_7$, ICDD card: 00-038-0440) precipitated out in the GC along with CE and OE. PE predominantly crystallized from the glass 3a at all the investigated temperatures, along with quartz (ICDD card 01-081-1665, marked as *Q*) as secondary phase. The intensity of the XRD peaks of PE and quartz were reduced at 1100 °C, likely due to dissolution effect in liquid phase.

According to the RT-XRD results, CE and OE crystallized out from glass 2a at 800 °C while quartz precipitated out as secondary phase after sintering at 900 °C and 1000 °C. Since, no peak for quartz was observed in HT-XRD results of glass 2a at 900 °C and 1000 °C; it can be assumed that the latter precipitated from liquid phase during cooling. Glass 3a was XRD amorphous after heat treatment at 800 °C, while PE and CE were the predominant phases after heat treatment at 900 °C along with yttrium silicate ($Y_2Si_2O_7$, ICDD card 00-045-0043, marked as YS) and keivyite as secondary phases. The conversion of PE to CE during cooling has been well documented in literature [2,29]. It is worth noting that YS is orthorhombic while K is monoclinic polymorph of $Y_2Si_2O_7$. A complex XRD pattern was obtained for GC 3a after heat treatment at 1000 °C. CE no more existed at this temperature and PE was the only predominant phase along with the presence of yttrium oxide borate silicate ($Y_{9.73}Y_6((SiO_4)_{4.8}(BO_4)_{1.2})O_2$, ICDD card 00-053-0055, marked as YBSi) and barium silicon oxide ($Ba_2Si_2O_5$, ICDD card 04-009-3348, marked as BaSi) as secondary phases. In addition to the crystalline phases identified, there were some unidentified XRD peaks in GCs 2a ($2\theta = 31.68^\circ$) and 3a ($2\theta = 27.93^\circ$ and 30.88°) after heat treatment at 1000 °C. Assuming that no barium or boron containing phases were observed by HT-XRD analysis of composition 3a, precipitation of YBSi and BaSi may be suggested to occur from the liquid phase components and at the expense of CE.

The RT-XRD spectrum of composition 2b was highly amorphous after heat treatment at 800 °C, with the presence of very low intensity peaks attributed to CE. However, in accordance with the HT-XRD results, both CE and OE were registered at 900 °C and 1000 °C with no significant alterations in the peak intensities of the $MgSiO_3$-polymorphs. In case of composition 3b, low intensity peaks for hexacelsian (ICDD: 01-088-1051, designated as HC) and CE registered among amorphous halo after heat treatment at 800 °C. However, with further increase in temperature to 900 °C, HC crystallized out extensively from the glassy matrix along with all the three $MgSiO_3$-polymorphs (CE, OE and PE), featuring peaks of less intensity (particularly PE). No major differences were observed in the XRD diffractograms of glass 3b after heat treatment at 1000 °C. These results are in agreement with data received from the HT-XRD analysis in which the same crystalline phase assemblage was registered.

From the technological application point of view, compositions 2b and 3b seem to be more promising as the GCs produced from these composition show good sintering ability and mechanical strength [6]. Particularly, the absence of metastable PE in GC 2b may be considered as an important step towards the prevention from aging of steatite ceramics and the increasing stability of the system during exploitation. The suggested Y-substitution for Mg in 2b [6] causes stabilization of OE and CE while Al_2O_3 affects the diffusion mechanism in the glass powder compacts resulting in well sintered $MgSiO_3$-based glass-ceramics. However, further experimentation, especially electrical resistivity measurements, on these two GCs compositions is required in order to validate our claims.

For all the samples characterized by XRD methods, infrared spectra were recorded, which are essential for distinguishing different stages of the thermal history. Those spectra reproduced in Fig. 7 are in accordance with the XRD results. The FTIR spectrum of all the enstatite based glasses (Fig. 1) shows the existence of four pronounced broad bands, which re-appear, characteristically modified, in all subsequent spectra of the respective GCs (Fig. 7). It is worth noting that composition 3a was XRD amorphous after heat treatment at 800 °C which is also supported by the appearance of broad bands in the IR spectra of

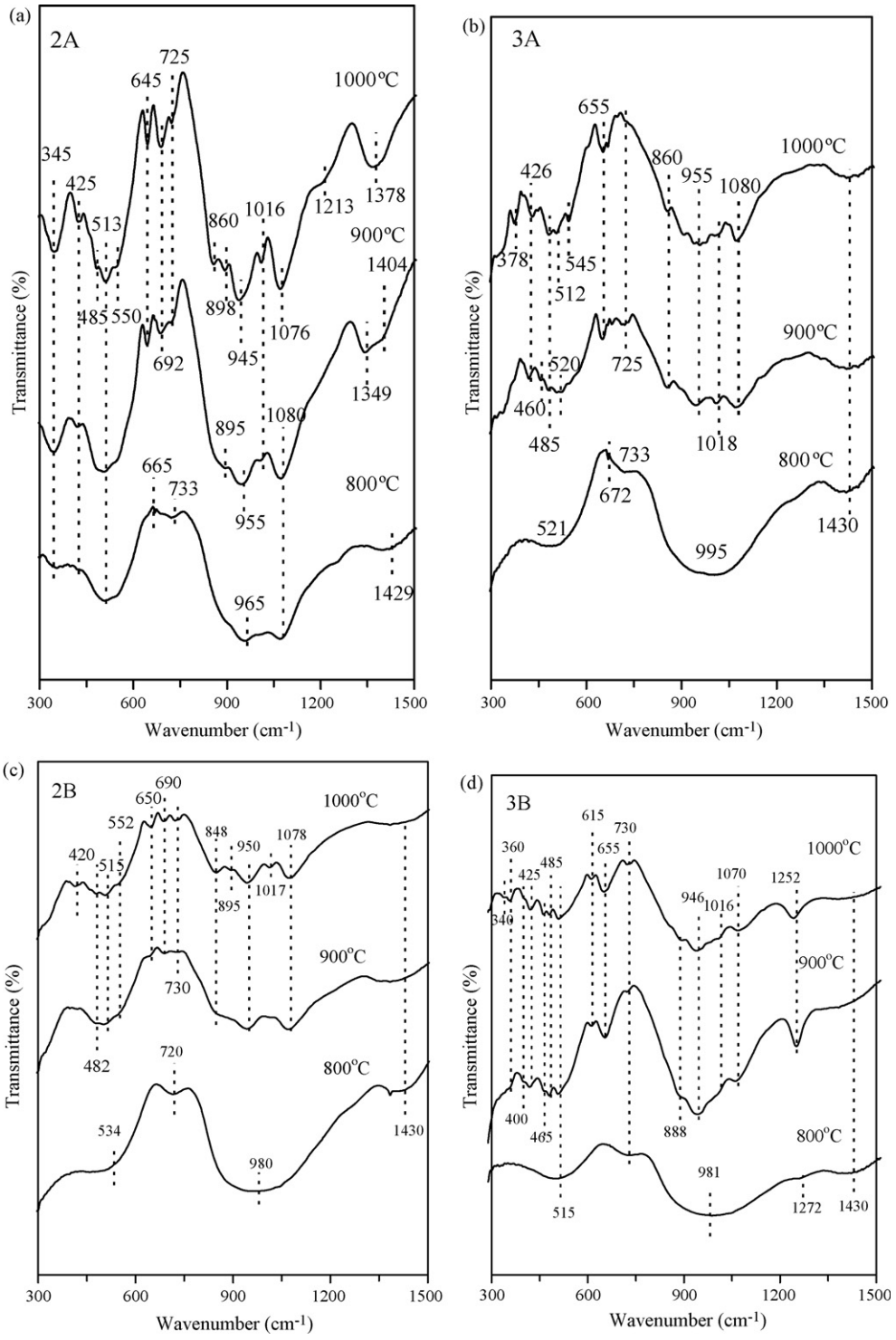

Fig. 7. FTIR spectra of all the glass powder compacts heat treated at (a) 800 °C (1073 K), (b) 900 °C (1173 K) and (c) 1000 °C (1273 K). Spectra were recorded by crushing the sintered GCs to powder form and mixing the GC powder with KBr.

the corresponding composition, however, the IR spectra features an additional band at 672 cm^{-1}, indicating the initiation of crystallinity in the glass (Fig. 7b). Despite of the different crystalline phase assemblage in all the compositions, no significant differences could be observed in their FTIR spectra at different temperatures. The multi-component bands in the region 1100–800 cm^{-1} indicate the mineralogical complexity of these GCs. Strong intense bands at ~1081 cm^{-1} and ~513 cm^{-1} can be interpreted as Si–O and Mg–O vibration modes in enstatite with slight shifts in the matrix [30]. According to Bowey et al. [31], the most intense bands for pure enstatite appear at 1077 cm^{-1}, 1014 cm^{-1}, 937 cm^{-1} and 856 cm^{-1}. Weaker peaks occur between these bands at 1149 cm^{-1}, 1108 cm^{-1} (shoulder), 1032 cm^{-1}, 974 cm^{-1} and 903 cm^{-1}. Bands for enstatite in the

region 833–625 cm^{-1} were also confirmed to be in accordance with the previous studies [31] and were observed at 737 cm^{-1}, 726 cm^{-1}, 693 cm^{-1}, 682 cm^{-1} and 650 cm^{-1}. In accordance with the results of Bowey et al. [31], we observed bands in the investigated GCs (Fig. 7a–d) at ~1080 cm^{-1}, 1018 cm^{-1}, 945 cm^{-1}, 860 cm^{-1}, 898 cm^{-1}, 733 cm^{-1}, 725 cm^{-1}, 692 cm^{-1}, 672 cm^{-1}, and 645 cm^{-1}. All the intense bands in the region 850–1100 cm^{-1} observed in the present investigation shifted towards higher wave numbers, while those in the region 833–625 cm^{-1} shifted towards lower wave numbers, in comparison to those reported by Bowey et al. [31]. When compared to the weaker bands as reported in the literature [31], we observed a band only at ~898 cm^{-1}, which is a characteristic band for enstatite [31]. According to Bowey et al. [31], the weak peak at 1149 $cm^{-1}$and medium peak at 903 cm^{-1}, are seen only in the samples with Mg in excess of 87% and the 1032 cm^{-1} feature has been measured only in samples with less than 92% Mg. However, the existence of the peaks at 974 cm^{-1} and 693 cm^{-1} do not seem to depend on composition. Variation between individual spectra of similar composition may also depend on crystal structure (e.g. monoclinic or orthorhombic) or orientation in the crushed samples, but much more study is required to determine their origin. According to Koike et al. [32], the peak positions for CE and OE are at ~500 cm^{-1}, which are in agreement with our results. In conjunction with the above mentioned peaks, Tsai [33] observed peaks at 480 cm^{-1} and 468 cm^{-1}, which according to him belong to enstatite. In accordance with the results obtained by Tsai [33], we observed peaks at ~485 cm^{-1} and ~460 cm^{-1}. OE and CE show almost same spectral features in the mid-IR region up to about 250 cm^{-1}. While the far-IR region, they can be distinguished easily, because both enstatites have small but sharp and characteristic features in this region, such as two double bands at around 200 cm^{-1} and 140 cm^{-1} of OE and, a single band at 150 cm^{-1} of CE [32]. In addition to all the transmittance bands as discussed above, an additional band appeared at ~1250 cm^{-1} in GC 3b (Fig. 7d). This band evidences the existence of HC in the GCs [34]. According to Aronne et al. [34], the IR absorption bands for HC lie at 1223 cm^{-1}, 934 cm^{-1}, 662 cm^{-1}, 630 cm^{-1}, 570 cm^{-1}, 481 cm^{-1} and 460 cm^{-1}. Since all the bands except the one at ~1250 cm^{-1} are either very close or overlap with the bands of the enstatite, therefore, it is difficult to identify the other transmittance bands corresponding to HC in the collected IR spectra. According to Scanu et al. [35], the band centred at 1250 cm^{-1} may be ascribed to the intramolecular vibrations of AlO_4 and SiO_4 tetrahedra (stretching of the Al–O and Si–O bonds). For the convenience of readers, summary of transmittance bands observed in the investigated GCs along with their assignment, according to literature is presented in Table 6.

Table 6
Assignment of FTIR bands in the investigated GCs.

Wave number (cm^{-1})	Assignment
1080, 1018, 945, 860, 898, 733, 725, 692, 645, 513, 485, 460	Enstatite
1250	Hexacelsian
1300–1500	B–O vibrations in [BO_3] triangle

4. Conclusions

The structural features and crystallization behaviour of enstatite based glasses has been studied. The infrared spectroscopy reveals that the symmetric and the anti-symmetric stretching modes of the Si–O–Si bonds of the Q_n units in the glass silicate network are distributed around Q_2 and Q_3. The addition of BaO and Al_2O_3 causes a change in the proportion of Q_2 and Q_3 units, which leads to a decease in the connectivity of the silicate glass network. The value of Avrami parameter, n calculated for Al_2O_3-free glasses indicates that surface nucleation and crystallization mechanism dominates, while according to the value of kinetic fragility index (F) these glasses feature lower glass-forming tendency in comparison to diopside based glasses.

The suggested Y-substitution for Mg in composition 2b causes stabilization of OE and CE, while addition of Al_2O_3 affects the diffusion mechanism in the glass powder compacts resulting in well sintered $MgSiO_3$-based GCs. The poor sintering ability of Al_2O_3-free glasses, 2a and 3a, has been attributed to their higher activation energy of viscous flow. CE and OE are the predominant phases in the GCs 2a while BaO stabilizes PE in GCs 3a. Addition of Al_2O_3 in glass 3b led to the formation of HC along with PE, CE and OE. FTIR results of the GCs are in accordance with the XRD results. The FTIR spectra of composition 3a showed an initiation of crystallinity after sintering at 800 °C. We could not separate the IR bands for OE and CE as both the crystalline phases show similar bands in the mid-IR region.

Acknowledgements

This study was financially supported by FCT, Portugal (Ashutosh Goel, Project no. SFRH/BD/37037/2007) and Swedish Institute, Sweden. Authors would also like to thank Ms. Annika Eriksson for her assistance in performing XRD and DSC experiments.

References

[1] J.V. Smith, Crystal structure and stability of the $MgSiO_3$ polymorphs: Physical properties and phase relations of Mg, Fe pyroxens, Miner. Soc. Am. Spec. Pap. 2 (1969) 3–29.
[2] W.E. Lee, A.H. Heuer, On the polymorphism of enstatite, J. Am. Ceram. Soc. 70 (1987) 349–360.
[3] W.L. Brown, N. Moromoto, J.W. Smith, A structural explanation of the polymorphism and transition of $MgSiO_3$, J. Geol. 69 (1961) 609–616.
[4] A.J. Perrotta, D.J. Stephenson, Clinoenstatite: high-low inversion, Science 148 (1965) 1090–1091.
[5] W. Mielcarek, D. Nowak-Wozny, K. Prociow, Correlation between $MgSiO_3$ phases and mechanical durability of steatite ceramics, J. Eur. Ceram. Soc. 24 (2004) 3817–3821.
[6] A. Goel, D.U. Tulyaganov, S. Agathopoulos, J.M.F. Ferreira, The role of Al_2O_3 on the sintering and crystallization of $MgSiO_3$ based glasses, Ceram. Int. 34 (2008) 505–510.
[7] W.A. Weyl, Coloured Glasses, vol. 558, Society of Glass Technology, 1951 (fifth reprint 1999) ISBN 0-900683-06X.
[8] G. Calas, L. Cormier, L. Galoisy, P. Jollivet, Structure–property relationships in multicomponent oxide glasses, C. R. Chim. 5 (2002) 831–843.
[9] S.-L. Lin, C.-S. Hwang, Structures of CeO_2–Al_2O_3–SiO_2 glasses, J. Non-Cryst. Solids 202 (1996) 61–67.

[10] J.T. Kohli, J.E. Shelby, J.S. Frye, A structural investigation of yttrium aluminosilicate glasses using Si-29 and Al-27 magic angle spinning nuclear-magnetic-resonance, Phys. Chem. Glasses 33 (1992) 73–78.
[11] M.I. Ojovan, W.E. Lee, An Introduction to Nuclear Waste Immobilisation, Elsevier Science Ltd., UK, 2005, (Chapter 17).
[12] L. Stoch, M. Sroda, Infrared spectroscopy in the investigation of oxide glasses structure, J. Mol. Struct. 511–512 (1999) 77–84.
[13] A. Goel, D.U. Tulyaganov, V.V. Kharton, A.A. Yaremchenko, S. Agathopoulos, J.M.F. Ferreira, The influence of BaO on the phase formation and properties of aluminous clinopyroxenes in the Diopside-Ca-Tschermak system, J. Am. Ceram. Soc. 90 (2007) 2236–2244.
[14] A. Goel, D.U. Tulyaganov, S. Agathopoulos, M. Ribeiro, J.M.F. Ferreira, Crystallization behavior of the glasses, structure and properties of sintered glass-ceramics in the Diopside-Ca-Tschermak system, J. Eur. Ceram. Soc. 27 (10) (2007) 3231–3238.
[15] A. Goel, D.U. Tulyaganov, V.V. Kharton, A.A. Yaremchenko, J.M.F. Ferreira, The effect of Cr_2O_3 on the crystallization behaviour and properties of La_2O_3 containing diopside glasses and glass-ceramics, Acta Mater. 56 (13) (2008) 3065–3076.
[16] S. Mahadevan, A. Giridhar, A.K. Singh, Calorimetric measurements on as-sb-se glasses, J. Non-Cryst. Solids 88 (1986) 11–34.
[17] O.A. Lafi, M.M.A. Imran, M.K. Abdullah, Glass transition activation energy. glass-forming ability and thermal stability of $Se_{90}In_{10-x}Sn_x$ ($x = 2$, 4, 6 and 8) chalcogenide glasses, Physica B 395 (2007) 69–75.
[18] A. Goel, E.R. Shabaan, D.U. Tulyaganov, J.M.F. Ferreira, Study of crystallization kinetics in glasses along the diopside-Ca-Tschermak join, J. Am. Ceram. Soc. 91 (2008) 2690–2697.
[19] A. Goel, D.U. Tulyaganov, S. Agathopoulos, M.J. Ribeiro, J.M.F. Ferreira, Synthesis and characterization of $MgSiO_3$-containing glass-ceramics, Ceram. Int. 33 (2007) 1481–1487.
[20] K. Chebli, J.M. Saiter, J. Grenet, A. Hamou, G. Saffarini, Strong-fragile glass forming liquid concept applied to GeTe chalcogenide glasses, Physica B 304 (2001) 228–236.
[21] M.M. Wakkad, E.Kh. Shokr, S.H. Mohamed, Optical and calorimetric studies of Ge–Sb–Se glasses, J. Non-Cryst. Solids 265 (2005) 157–166.
[22] T.A. Vilgis, Strong and fragile glasses: a powerful classification and its consequences, Phys. Rev. B 47 (1993) 2882–2885.
[23] R. Böhmer, C.A. Angell, Global and local relaxations in glass-forming materials, in: R. Richert, A. Blumen (Eds.), Disorder Effects on Relaxational Processes, Springer, Berlin, Heidelberg, 1994, pp. 11–54.
[24] W.A. Johnson, K.F. Mehl, Reaction kinetics in processes of nucleation and growth, Trans. Am. Inst. Mining Eng. 135 (1939) 416–442.
[25] M. Avrami, Kinetics of phase change. I General theory, J. Chem. Phys. 7 (1939) 1103–1112;
M. Avrami, Kinetics of phase change. II Transformation-Time relations for random distribution of nuclei, J. Chem. Phys. 8 (1940) 212;
M. Avrami, Granulation, phase change, and microstructure kinetics of phase change. III, J. Chem. Phys. 9 (1941) 177–184.
[26] A. Goel, E.R. Shabaan, F.C.L. Melo, M.J. Ribeiro, J.M.F. Ferreira, Non-isothermal crystallization kinetic studies on $MgO–Al_2O_3–SiO_2–TiO_2$ glass, J. Non-Cryst. Solids 353 (2007) 2383–2391.
[27] A. Goel, E.R. Shabaan, F.C.L. Melo, M.J. Ribeiro, J.M.F. Ferreira, Influence of NiO on the crystallization kinetics of near stoichiometric cordierite glasses nucleated with TiO_2, J. Phys. Condens. Mat. 19 (2007) 386231.
[28] J. Vázquez, C. Wagner, P. Villares, R. Jiménez-Garay, Glass transition and crystallization kinetics in $Sb_{0.18}As_{0.34}Se_{0.48}$ glassy alloy by using non-isothermal techniques, J. Non-Cryst. Solids 235–237 (1998) 548–553.
[29] L.M. Echeverria, G.N. Beall, Enstatite ceramics; glass and gel routes, in: K.M. Nair (Ed.), Glasses for Electronic applications, Ceramic Transactions, vol. 20, American Ceramic Society, Westerville, OH, 1991 pp. 235–244.
[30] K. Nakamoto, Infrared and Raman Spectra of Inorganic and Coordination Compounds, 3rd ed., John Wiley & Sons, New York, 1978 pp. 105–194, 239–249.
[31] J.E. Bowey, A. Morlok, M. Kohler, M. Grady, 2–16 μm spectroscopy of micron-sized enstatite $(Mg,Fe)_2Si_2O_6$ silicates from primitive chondritic meteorites, Mon. Not. R. Astron. Soc. 376 (2007) 1367–1374.
[32] C. Koike, A. Tsuchiyama, H. Shibai, H. Suto, T. Tanabe, H. Chihara, H. Sogawa, H. Mouri, K. Okada, Absorption spectra of Mg-rich Mg-Fe and Ca pyroxenes in the mid- and far-infrared regions, Astron. Astrophys. 363 (2000) 1115–1122.
[33] M.-T. Tsai, Synthesis of nanocrystalline enstatite fiber via alkoxide sol–gel process, J. Am. Ceram. Soc. 88 (2005) 1770–1772.
[34] A. Aronne, S. Esposito, C. Ferone, M. Pansini, P. Pernice, FTIR study of the thermal transformation of barium-exchanged zeolite A to celsian, J. Mater. Chem. 12 (2002) 3039–3045.
[35] T. Scanu, J. Guglielmi, Ph. Colomban, Ion-exchange and hot corrosion of ceramic composites matrices—a vibrational and microstructural study, Solid State Ionics 70–71 (1994) 109–120.